Effects of Strain and Film Thickness on the Stability of the Rhombohedral Phase of HfO_2

Yuke Zhang,[1] Qiong Yang,[1,2,*] Lingling Tao,[3] Evgeny Y. Tsymbal,[3,†] and Vitaly Alexandrov[2,‡]

[1] *School of Materials Science and Engineering, Xiangtan University, Xiangtan, Hunan 411105, China*
[2] *Department of Chemical and Biomolecular Engineering, University of Nebraska, Lincoln, Nebraska 68588, USA*
[3] *Department of Physics and Astronomy, University of Nebraska, Lincoln, Nebraska 68588, USA*

(Received 22 January 2020; Received 10 Jane 2020; accepted 11 June 2020; published 22 July 2020)

The discovery of ferroelectric polarization in HfO_2-based ultrathin films has spawned much interest due to their potential applications in data storage. In 2018, an $R3m$ rhombohedral phase was proposed to be responsible for the emergence of ferroelectricity in the [111]-oriented $Hf_{0.5}Zr_{0.5}O_2$ thin films, but the fundamental mechanism of ferroelectric polarization in such films has remained poorly understood. In this paper, we employ density-functional-theory calculations to investigate structural and polarization properties of the $R3m$ HfO_2 phase. We find that the film thickness and in-plane compressive-strain effects play a key role in stabilizing the $R3m$ phase, leading to robust ferroelectricity of [111]-oriented $R3m$ HfO_2.

DOI: 10.1103/PhysRevApplied.14.014068

I. INTRODUCTION

HfO_2-based materials have aroused much interest in recent years due to their promise in nanoelectronics [1–5]. Compared with conventional perovskite ferroelectrics, HfO_2-based ferroelectric thin films exhibit a range of properties that are appealing for low-power high-density memory applications [6,7], such as compatibility with silicon-based semiconductor technology, robust switchable ferroelectricity at the nanoscale (<10 nm), and a large band gap of about 5–6 eV.

The atomistic origin for the emergence of switchable ferroelectric polarization in HfO_2-based ultrathin films, however, remains unclear [8]. The ground-state monoclinic $P2_1/c$ phase of HfO_2 is centrosymmetric, and thus, does not support ferroelectric polarization. Therefore, considerable prior efforts have been focused on identifying a ferroelectric HfO_2 phase that is stable and displays pronounced ferroelectricity at the nanoscale, as observed experimentally [3,8–11]. For example, by employing a group theoretical analysis, in combination with density-functional-theory (DFT) calculations, Huan *et al*. have previously identified two noncentrosymmetric polar orthorhombic phases with $Pca2_1$ and $Pmn2_1$ space groups that could be responsible for ferroelectricity in HfO_2-based films [8]. In particular, the $Pca2_1$ phase is most widely accepted as the ferroelectricity origin, based on numerous experimental and theoretical studies [3,8–11], which is also found to exhibit sizable spin-orbit coupling [12] and magnetoelectric effects at the ferroelectric-ferromagnetic interface based on DFT calculations [13]. However, the phases $Pca2_1$ and $Pmn2_1$ are less stable thermodynamically than that of monoclinic $P2_1/c$ in the bulk. Though many factors, such as strain (stress) [11,14,15], doping [16–18], defects [19], electric field [20], and surface energy [21], are found to be helpful for the stabilization of the orthorhombic $Pca2_1$ ferroelectric phase, a convincing and widely accepted mechanism for the stability of the possible ferroelectric phase of HfO_2-based thin films is still required.

Recently, Wei *et al*. reported a rhombohedral ferroelectric phase with $R3m$ space group, which is different from previously described polar orthorhombic phases [22]. The $R3m$ phase is identified by using a combination of x-ray diffraction and transmission electron microscopy in the predominantly [111]-oriented $Hf_{0.5}Zr_{0.5}O_2$ thin film epitaxially grown on the $La_{0.7}Sr_{0.3}MnO_3/SrTiO_3$ substrate. One of the structural features of the observed phase is that the atomic plane spacing along the out-of-plane direction (d_{111}) is markedly larger than that along the [−111], [1−11], and [11−1] directions ($d_{-111}=d_{1-11}=d_{11-1}$) that are consistent with a rhombohedral unit cell. The remnant polarization (P_r) reaches a significant value of 34 $\mu C/cm^2$ for the $Hf_{0.5}Zr_{0.5}O_2$ film thickness of about 5 nm. However, according to DFT calculations, the total energy of the rhombohedral $R3m$ phase turns out to be even higher than that for orthorhombic $Pca2_1$. Moreover, substantial strain is required for HfO_2 (or $Hf_{0.5}Zr_{0.5}O_2$) to display ferroelectric polarization comparable with experimental values.

*qyang@xtu.edu.cn
†tsymbal@unl.edu
‡valexandrov2@unl.edu

 © 2020 American Physical Society

It is also observed experimentally that both the polarization magnitude and d_{111}–d_{11-1} difference for the rhombohedral ferroelectric thin film increase upon decreasing the film thickness, which is important for the application of nanoscale HfO_2-based ferroelectrics. These experimental findings stimulate our present study, focusing on the behavior of the identified $R3m$ ferroelectric phase through the analysis of strain and size effects.

Here, we employ DFT calculations to provide further insights into the origin of ferroelectric polarization and phase stability of the $R3m$ ferroelectric polymorph of HfO_2. To this end, we focus on the experimentally relevant system of [111]-oriented HfO_2 thin films and analyze both strain and size effects. We find that an in-plane compressive strain is essential for reproducing the experimentally observed d_{111}–d_{11-1} difference and polarization enhancement in the [111]-oriented $R3m$ HfO_2 films. The size effect is also found to facilitate phase stabilization under in-plane compressive strain of the film. The calculated results provide insights into the emergence of stable ferroelectric polarization in HfO_2 thin films, which should be useful for a better understanding of the behavior of nanoscale ferroelectric films based on HfO_2.

II. COMPUTATIONAL METHODOLOGY

Here, we focus on the rhombohedral $R3m$, tetragonal $P4_2/nmc$, ferroelectric orthorhombic $Pca2_1$, and nonferroelectric monoclinic $P2_1/c$ phases of HfO_2 (see Ref. [20] for more details on the $P4_2/nmc$, $Pca2_1$, and $P2_1/c$ HfO_2 phases). All DFT calculations are performed using the projector-augmented-wave (PAW) method, as implemented in the Vienna *ab initio* simulation package (VASP) code [23]. The Perdew-Burke-Ernzerhof generalized gradient approximation (GGA PBE) is used to describe exchange-correlation interactions [24]. The plane-wave cutoff energy is chosen to be 450 eV. The atomic coordinates of the $R3m$ phase are taken from Ref. [22]. The strain effect on ferroelectric polarization and phase stability of bulk HfO_2 is examined using hexagonal cells (12 Hf and 24 O atoms) with their [0001] directions along the [111] directions of conventional unit cells (4 Hf and 8 O atoms). The [111]-oriented periodic slabs are constructed with a vacuum gap of at least 18 Å in the out-of-plane direction. The $5 \times 5 \times 4$ and $5 \times 5 \times 1$ Monkhorst-Pack k-point meshes [25] are used for the bulk and thin-film calculations, respectively, to ensure energy convergence. Structural optimizations are carried out until the Hellmann-Feynman forces on each atom are less than 5 meV/Å. The magnitude of ferroelectric polarization for the $R3m$ phase is calculated within the Berry phase approach by taking the cubic $Fm3m$ phase as the nonpolar reference state [26].

III. RESULTS AND DISCUSSION

Figures 1(a) and 1(b) show the atomic structure and lattice vectors, respectively, of the $R3m$ rhombohedral phase of HfO_2 in its conventional unit cell (with 4 Hf and 8 O atoms). The hexagonal cell of rhombohedral $R3m$ HfO_2 (with 12 Hf and 24 O atoms), which is employed to examine the strain effects, is depicted in Fig. 1(c) with its out-of-plane direction along the [111] direction of the conventional unit cell [Figs. 1(a) and 1(b)]. The calculated lattice constants, a and c, of the stress-free hexagonal cell of $R3m$ HfO_2 are 7.184 and 8.810 Å, respectively. While there are no available experimental lattice constants for bulk $R3m$ HfO_2 for comparison, the chosen computational scheme utilizing the PBE functional provides good agreement between the computed and experimental [22] interplanar crystal spacing. In our simulations, the equiaxial strain is applied on the (001) plane of the hexagonal cell [i.e., the (111) plane of a conventional cell, as shown in Fig. 1(b)] with the out-of-plane lattice fully relaxed to stress-free, to be consistent with previous experimental work [22]. Figure 1(d) shows the change of the d spacing as a function of the in-plane compressive strain. Under the strain-free conditions, the conventional unit cell of $R3m$ HfO_2 shown in Fig. 1(a) is nearly cubic, with $d_{111} \approx d_{11-1}$ ($d_{-111} = d_{1-11} = d_{11-1}$). When the in-plane strain is increased, d_{111} gradually goes up and d_{11-1} goes down [see Fig. 1(d)]. According to the scanning transmission electron microscopy (STEM) measurements, d_{111} for the $R3m$ $Hf_{0.5}Zr_{0.5}O_2$ phase ranges between 2.98 and 3.27 Å for film thicknesses between 9 and 1.5 nm [22]. From the d_{111}-strain relation for HfO_2 [Fig. 1(d)] found in this work, the in-plane compressive strain is estimated to be between 1.5 and 5% to provide experimentally measured values of d_{111}.

Using this experimentally relevant range of compressive strains, we then calculate the out-of-plane spontaneous polarization (P), as plotted in Fig. 1(e). It is clearly seen that polarization is small for the in-plane strain below 3%, while it increases rapidly beyond 3% and reaches about 25 $\mu C/cm^2$ at 5% strain. This result is in full agreement with the DFT-computed polarization of the $R3m$ phase of $Hf_{0.5}Zr_{0.5}O_2$ as a function of d_{111} reported previously [22]. Thus, we conclude that a large in-plane strain is needed for $R3m$-phase HfO_2 to exhibit a pronounced ferroelectric polarization.

We next provide insights into the origin of the increase of polarization as a function of strain for the $R3m$ phase of HfO_2. To this end, we first examine the atomic structures of the strain-free and compressively strained $R3m$ phase. For the strain-free case shown in Fig. 1(c), every O atom is coordinated with four Hf atoms to form an O-Hf_4 tetrahedron. This atomic structure is similar to that of the nonpolar tetragonal $P4_2/nmc$ phase, and therefore, the spontaneous polarization of the stress-free

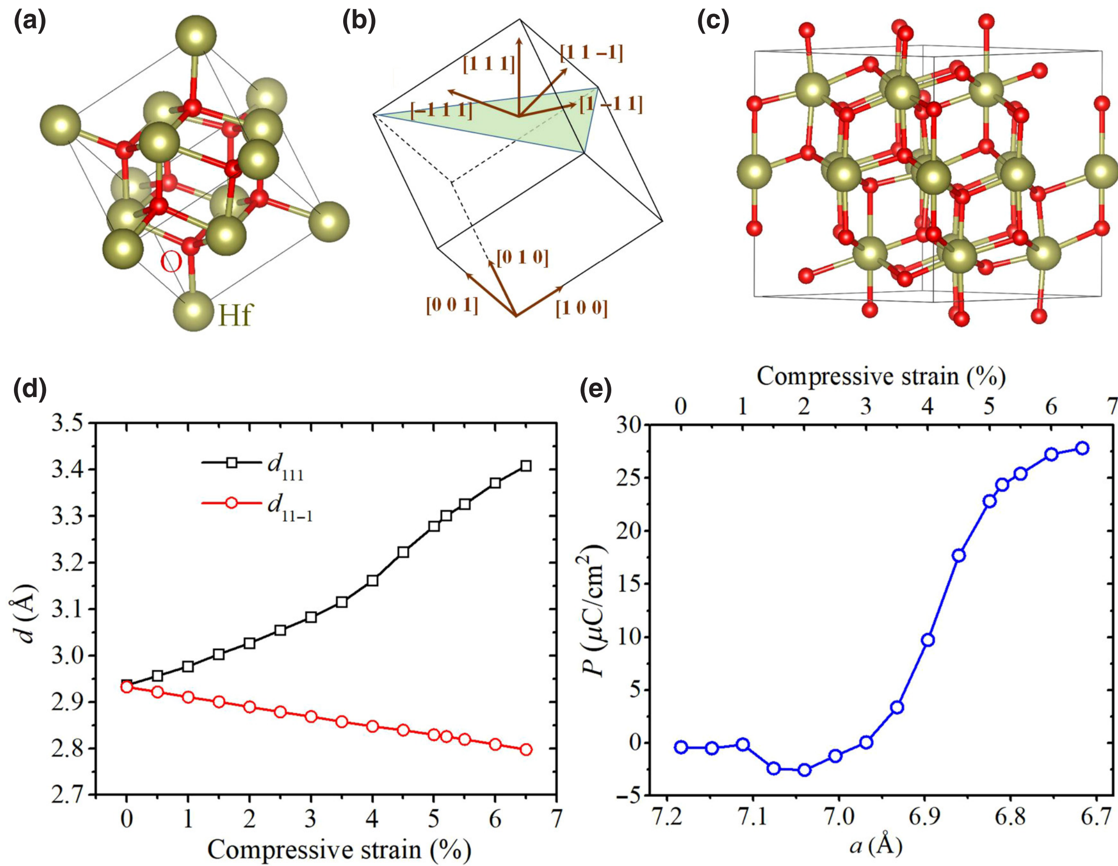

FIG. 1. Atomic structure (a) and lattice vectors (b) of $R3m$-phase HfO_2 in conventional cell. (c) Atomic structure of the [111]-oriented $R3m$ phase in hexagonal cell. (d) The d spacing (d) of $R3m$-phase HfO_2 versus in-plane compressive strain. (e) Spontaneous polarization (P) of strained $R3m$-phase HfO_2. Upper and lower horizontal coordinates show the magnitudes of in-plane compressive strain and lattice constants, respectively. Atomic structures are plotted using VESTA software.

rhombohedral $R3m$ phase is negligible. For strained $R3m$ HfO_2 (Fig. 2), we observe that, due to the in-plane compression and out-of-plane extension, the vertical Hf—O bonds become contracted and elongated, respectively, relative to the strain-free case. Specifically, by inspecting Hf-O_2 layers of the strained compound, we find that one of the four O atoms above Hf forms the O-Hf_4 tetrahedron with the upper Hf-O_2 layer, while three of the four O atoms below Hf form the O-Hf_4 tetrahedron with the lower Hf-O_2 layer. This bonding order causes structural asymmetry and leads to polarization pointing upward in strained $R3m$ HfO_2.

The structural changes induced by the in-plane strain can be quantified by computing the bond-length variations for the vertical Hf—O bonds. In $R3m$ HfO_2, there are two types of Hf—O bonds in the vertical direction, as shown in Fig. 2(a). For the primary Hf—O bonding order, denoted by the dashed ellipse in Fig. 2(a), the upper Hf—O bonds are shorter than the lower ones. It is seen that under stress the length of the upper (shorter) Hf—O bonds remains almost constant, whereas the length of the lower (longer) Hf—O bonds increases substantially as the strain goes from 3%to 5% [red open circles in Fig. 2(b)]. This is consistent with the observed polarization enhancement under the in-plane strain shown in Fig. 1(e). The trend for the behavior of the second type of the Hf—O bonds, denoted by the dashed rectangle in Fig. 2(a), is opposite to that of the primary bonding order. Since the length of the upper (longer) Hf—O bonds with the secondary bonding order begins increasing rapidly when the strain reaches 1.5% [blue solid squares in Fig. 2(b)], a very small negative polarization can be seen in Fig. 1(e) under this strain.

Next, we analyze the charge-density redistribution under different in-plane strains. Figures 2(c) and 2(d) show the computed electron densities of strain-free and 6% compressively strained $R3m$ HfO_2, respectively, across the (110) plane of the hexagonal cell. It can be seen that, in the 6% compressively strained case, the electron density between Hf and the lower O atoms marked by the dashed ellipses (primary Hf—O bonding order) in Fig. 2(d) becomes depleted compared with that of the strain-free case due to considerable elongation of these Hf—O bonds. Thus, it is determined that ferroelectric polarization

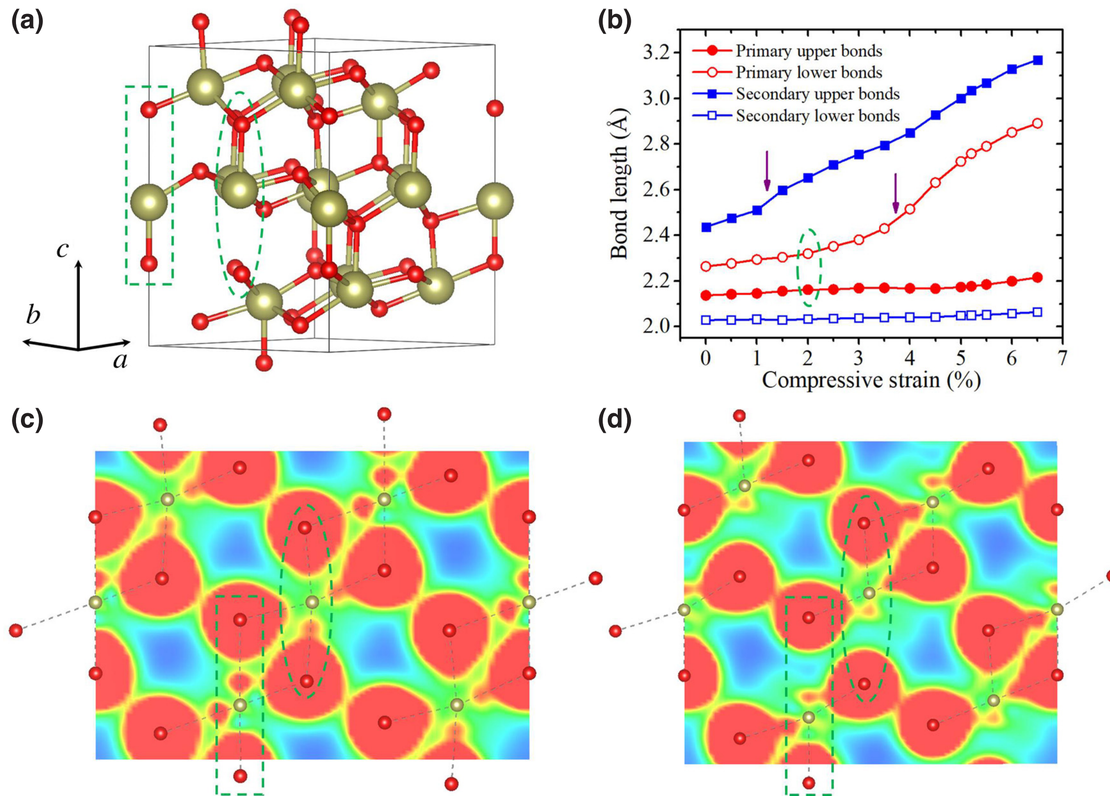

FIG. 2. (a) Atomic structure of 6% compressively strained [111]-oriented $R3m$ HfO_2 plotted using VESTA software. Two types of Hf—O bonds are indicated by the dashed ellipse and rectangle. (b) Hf—O bond length for the two types of bonds as a function of compressive strain, with vertical arrows marking the positions of a rapid increase of the bond lengths. Charge densities of strain-free (c) and compressively strained (d) $R3m$ HfO_2 along the (110) plane of the hexagonal cells.

of the compressively strained [111]-oriented $R3m$ HfO_2 phase originates from the disruption of the Hf—O bonding order, which is similar to that of perovskite-structured ferroelectrics, such as $BaTiO_3$ and $PbTiO_3$ [27,28]. The same electron density depletion is also found between Hf and the upper O atoms marked by the dashed rectangle (secondary Hf—O bonding order) in Fig. 2(d), which have weak and opposite contributions to that of the main polarization."

It is known from previous DFT calculations that the energy of $R3m$ HfO_2 lies above the ground-state $P2_1/c$ bulk phase by almost 160 meV/f.u. [22]. It is also determined that the compressive strain required for pronounced ferroelectric polarization of [111]-oriented $R3m$ HfO_2 should be relatively high [~5%, Fig. 1(e)]. Therefore, we next examine how the stability of the bulk HfO_2 phases changes as a function of applied volumetric and in-plane stress. To this end, we consider tetragonal $P4_2/nmc$, orthorhombic ferroelectric $Pca2_1$, and the most-stable nonferroelectric monoclinic $P2_1$/c phases of HfO_2 and compare their stability with that of the $R3m$ phase. The volumetric stress is applied to a conventional cell of HfO_2 (with 4 Hf and 8 O atoms) by fixing the cell volume and fully relaxing the cell shape and atomic coordinates. Figure 3(a) shows the calculated phase-stability diagrams relative to the ground-state $P2_1/c$ phase under volumetric stress. It is seen that, regardless of the applied stress, the bulk $R3m$ HfO_2 phase turns out to be the highest-energy polymorph.

We next analyze the phase stability of the [111]-oriented HfO_2 films under the in-plane equiaxial strain [Fig. 3(b)]. The in-plane strains are imposed on the (001) planes of the constructed hexagonal cells (i.e., the {111} planes of the conventional cells, see Fig. 1) of the considered $R3m$, $P4_2/nmc$, $Pca2_1$, and $P2_1/c$ phases, with fixed lattice angles and fully relaxed out-of-plane lattice constants and all atomic positions. For each HfO_2 polymorph, there are four possible ⟨111⟩ crystal orientations ([111], [−111], [1−11], and [11−1] directions in conventional cells) that should be taken into consideration, when investigating the effects of epitaxial strain.

The monoclinic $P2_1/c$ phase displays the same energy when strain is applied in the planes perpendicular to the [111] and [1−11] directions, but exhibits different energies when strain is applied in the planes perpendicular to the [−111] and [11−1] directions. Also, the orthorhombic $Pca2_1$ and tetragonal $P4_2/nmc$ phases are characterized by the same energies when the in-plane strains are applied perpendicular to any of the ⟨111⟩ directions. For the rhombohedral $R3m$ phase, we only plot results for

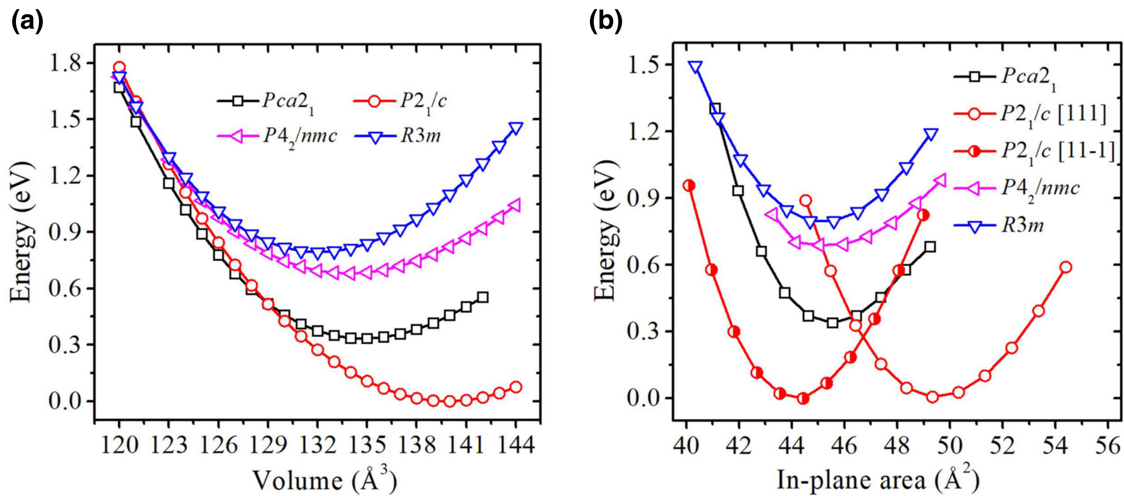

FIG. 3. (a) Total energies of different phases of HfO_2 in conventional cells (with 12 atoms) under volumetric strain. (b) Total energies of different phases of ⟨111⟩-oriented HfO_2 (per 12 atoms) under plane strain.

the [111]-oriented case, since strain imposed along the (11−1), (1−11), and (11−1) planes results in phase instability. Figure 3(b) shows the estimated energy variation upon changing the in-plane area of the hexagonal cells for the corresponding HfO_2 phases. It is seen from Fig. 3(b) that the $P2_1/c$ phase remains the most stable, and the $R3m$ phase is the least stable under the considered strains. We note here that Liu and Hanrahan previously found that the $Pca2_1$ and $Pbca$ phases were more stable than the $P2_1/c$ phase for [111]-oriented HfO_2 under compressive strain [14]. The disagreement with our results could be because the difference of the in-plane areas of the $P2_1/c$ phase with different ⟨111⟩ orientations was not considered in their study.

From the above calculation, the $R3m$ phase of HfO_2 is of higher energy than that of the other considered competing polymorphs under either volumetric strain or plane strain in the bulk form. Considering another experimentally observed fact that ferroelectric polarization of the $R3m$ HfO_2 film is more pronounced at smaller thicknesses [22], we further investigate the effect of thin-film size on the phase stability of [111]-oriented HfO_2. The ⟨111⟩-oriented HfO_2 thin films are constructed with the Hf-O_2 layer numbers (N) varying from one to nine, as shown in Fig. 4(a). In these calculations, both the lattice and atomic coordinates are allowed to fully relax to obtain stress-free configurations of the HfO_2 thin films for each phase. Although the symmetry of bulk phases is reduced for the corresponding films, we keep the same notation for both bulk and film phases. Figure 4(b) shows the total energy of a thin film normalized per one Hf-O_2 layer (4 Hf and 8 O atoms) as a function of film thickness across the three HfO_2 polymorphs. Overall, it is seen that the energies of the HfO_2 thin films increase upon reducing the film thickness for all phases, due to the increasing proportion of surface energy. The energy of the $P2_1/c$ phase increases rapidly when the

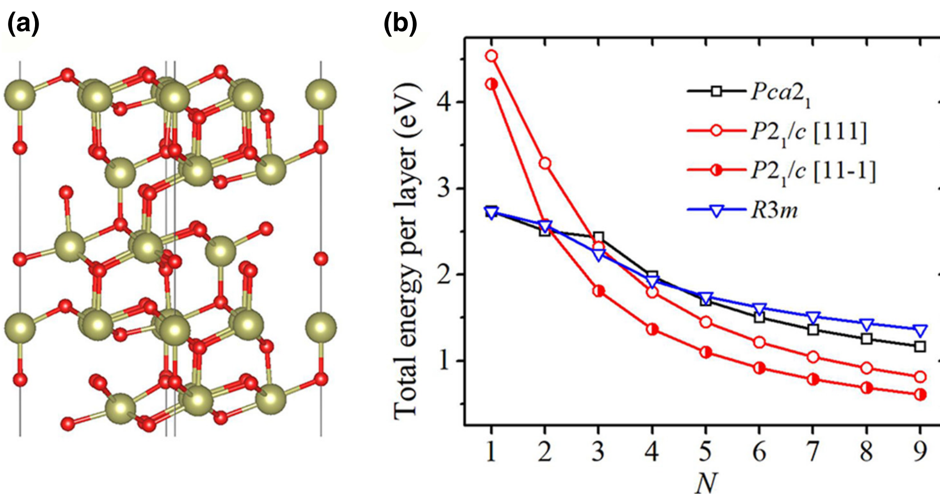

FIG. 4. (a) Atomic structure of [111]-oriented $R3m$-phase HfO_2 thin film with $N = 5$ plotted using VESTA software. (b) Total energies of different phases for ⟨111⟩-oriented HfO_2 thin films per Hf-O_2 layer. Total energy of stress-free bulk $P2_1/c$ HfO_2 per 12 atoms set to be zero. Since the $P4_2/nmc$ phase for many thicknesses is not stable, their energies are not given here. $Pca2_1$ phase is also not stable for $N = 1$ and 2.

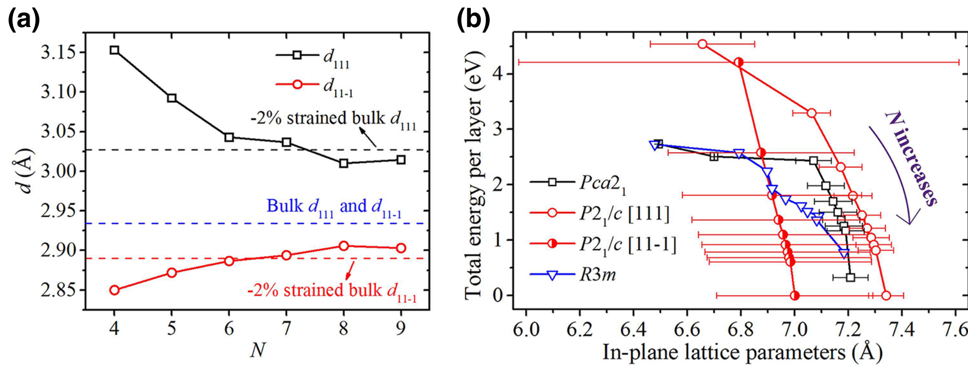

FIG. 5. (a) Average d_{111} and d_{11-1} of $R3m$ HfO_2 thin films with different thicknesses. (b) Total energies per Hf-O_2 layer and in-plane lattice constants of ⟨111⟩-oriented HfO_2 thin films with different thicknesses. Symbols on each line from the left to right denote $N=1$ to 9, and the last point is the data of bulk for each phase. Error bars denote length difference of the two in-plane lattices of each phase.

film thickness decreases from nine to one Hf-O_2 layers, while the variation of the energy for the $R3m$ phase is much slower. From the computed energies of thin-film and bulk HfO_2, the surface energies for $R3m$[111], $Pca2_1$[111], $P2_1/c$[111], and $P2_1/c$[11−1] are estimated at 2.48, 3.10, 3.65, and 2.79 eV per surface unit cell (i.e., 0.91, 1.10, 1.20, and 1.02 J/m^2), respectively, according to formula (3) of Ref. [29], where E_n is the total energy of the thin film with nine Hf-O_2 layers; ΔE_n is the energy difference between the thin films with eight and nine Hf-O_2 layers, and n equals the maximum Hf-O_2 layer number, which is nine. Generally, these surface energies of the {111} planes are much lower than those of the {100} planes in Ref. [21], which make the ⟨111⟩-oriented epitaxial growth of HfO_2 films more favorable. It is interesting to observe in Fig. 4(b) that the $R3m$ phase is more stable than that of the $Pca2_1$ phase if the film thickness is less than five Hf-O_2 layers. Moreover, $R3m$ HfO_2 becomes the most stable phase under extreme film thicknesses ($N=1$, 2). This suggests that the $R3m$ HfO_2 phase may be stabilized under the small thickness due to its lower surface energy displaying robust ferroelectric polarization.

We next discuss the structural properties of the ⟨111⟩-oriented HfO_2 thin films. First, the d spacing for the relaxed [111]-oriented $R3m$ HfO_2 thin films is analyzed. It is seen from Fig. 5(a) that d_{111} is larger than d_{11-1} for the $R3m$ HfO_2 films for all thicknesses considered in this study. The difference between d_{111} and d_{11-1} gradually increases with a decrease in the film thickness, which is in agreement with experimental data obtained for $Hf_{0.5}Zr_{0.5}O_2$ [22]. Figure 5(b) shows how the thin-film energies and the in-plane lattice constants change when the ⟨111⟩-oriented HfO_2 film thickness increases from $N=1$ to 9. It is seen that the in-plane lattice constants decrease and the average energies increase upon reducing the film thickness. The decrease in the in-plane lattice constant of $R3m$ HfO_2 with N is especially pronounced – it shrinks by almost 4% for the $N=4$ film relative to that of bulk $R3m$ HfO_2. This indicates that the in-plane compressive strain for the $R3m$ HfO_2 thin film is substantially facilitated by size effects. In Fig. 5(b), we also depict the difference between the two in-plane lattice constants for each phase through the error bars to show their in-plane structural asymmetry. It is seen that the two in-plane lattices are the same for the $R3m$ thin film, while the lengths for the two in-plane lattices for the [111]-oriented $Pca2_1$ and $P2_1/c$ phases are different. Furthermore, the difference in length for the two in-plane lattices for the [11−1]-oriented $P2_1/c$ phase is significant. The polarization magnitude of the thin films is not calculated in this paper due to the disadvantage of the Berry phase method in describing polarization of the film.

From existing experiments and present calculations, it is seen that a substantial in-plane strain (∼5%) is required for [111]-oriented $R3m$ HfO_2 to exhibit a noticeable polarization. From Fig. 5(b), it is expected that the $R3m$ phase would be favorable if the (doped) HfO_2 film were grown on a substrate with smaller in-plane lattice constants. Besides the epitaxial strain, the structural symmetry of the substrates is also believed to play an important role on the phase stability of the HfO_2 thin film from our calculations. The significant difference between the two in-plane lattice constants of the ⟨111⟩-oriented $P2_1/c$ HfO_2 thin film [shown in Fig. 5(b)], especially the [11−1]-oriented one, indicates that the $P2_1/c$ phase may be inhibited when the (doped) HfO_2 film is grown on a substrate with specific symmetry. Additionally, we believe that the interfacial effects and electrostatic screening from the electrode-HfO_2 interface can also be important factors for the stability of the $R3m$ phase, which have not been studied in this work, since electrostatic screening would weaken the depolarization electric field in the thin film and make the polar phase, such as $R3m$, more stable. Furthermore, the effects of doping and defects may also play important roles in the stability and ferroelectric polarization of the $R3m$ phase in practical HfO_2-based thin films.

IV. CONCLUSIONS

In summary, we examine the effects of strain and film thickness on the emergence of ferroelectricity in rhombohedral-phase-based HfO_2 thin films. Through the calculation of spontaneous polarization as a function of applied strain, we demonstrate that relatively large strain

(∼5%) is necessary for ferroelectric polarization of the $R3m$ phase to be comparable with the experimentally observed value. We find that, under the in-plane compressive strain, the [111]-oriented $R3m$ phase exhibits a vertical long and short Hf—O bonding order, which is the origin of significant ferroelectric polarization. However, the bulk $R3m$ phase is determined to be less stable than the ground-state $P2_1/c$ polymorph, regardless of the imposed volumetric or plane strains. Nevertheless, it is found that the $R3m$ phase becomes the most stable phase at extremely small thicknesses of thin films. The obtained results suggest that the $R3m$ phase responsible for the emergence of ferroelectricity in HfO_2 thin films can be stabilized under the combined effects of size and strain.

ACKNOWLEDGMENTS

This work is supported by the Research Foundation of Education Bureau of Hunan Province, China (Grants No. 18B056 and No. 19C1783), the National Natural Science Foundation of China (Grants No. 11932016 and No. 51902274), the National Science Foundation (NSF) through MRSEC (Grant No. DMR-1420645), and the EPMD (Grant No. ECCS-1917635) Programs. Q.Y. thanks the China Scholarship Council (CSC) for financial support.

[1] T. S. Böscke, J. Müller, D. Bräuhaus, U. Schröder, and U. Böttger, Ferroelectricity in hafnium oxide thin films, Appl. Phys. Lett. **99**, 102903 (2011).

[2] J. Müller, U. Schröder, T. S. Böscke, I. Müller, U. Böttger, L. Wilde, J. Sundqvist, M. Lemberger, P. Kücher, and T. Mikolajick, Ferroelectricity in yttrium-doped hafnium oxide, J. Appl. Phys. **110**, 114113 (2011).

[3] J. Muller, T. S. Böscke, U. Schröder, S. Mueller, D. Brauhaus, U. Bottger, L. Frey, and T. Mikolajick, Ferroelectricity in simple binary ZrO_2 and HfO_2, Nano Lett. **12**, 4318 (2012).

[4] T. Mikolajick, S. Slesazeck, M. H. Park, and U. Schroeder, Ferroelectric hafnium oxide for ferroelectric random-access memories and ferroelectric field-effect transistors, Mrs. Bull. **43**, 340 (2018).

[5] B. Zeng, W. Xiao, J. Liao, H. Liu, M. Liao, Q. Peng, S. Zheng, and Y. Zhou, Compatibility of HfN metal gate electrodes with $Hf_{0.5}Zr_{0.5}O_2$ ferroelectric thin films for ferroelectric field-effect transistors, IEEE Electron. Device Lett. **39**, 1508 (2018).

[6] A. Chernikova, M. Kozodaev, A. Markeev, D. Negrov, M. Spiridonov, S. Zarubin, O. Bak, P. Buragohain, H. Lu, and E. Suvorova, Ultrathin $Hf_{0.5}Zr_{0.5}O_2$ ferroelectric films on Si, ACS Appl. Mater. Interfaces **8**, 7232 (2016).

[7] X. Tian, S. Shibayama, T. Nishimura, T. Yajima, S. Migita, and A. Toriumi, Evolution of ferroelectric HfO_2 in ultrathin region down to 3nm, Appl. Phys. Lett. **112**, 102902 (2018).

[8] T. D. Huan, V. Sharma, G. A. Rossetti Jr, and R. Ramprasad, Pathways towards ferroelectricity in hafnia, Phys. Rev. B **90**, 064111 (2014).

[9] S. Clima, D. J. Wouters, C. Adelmann, T. Schenk, U. Schroeder, M. Jurczak, and G. Pourtois, Identification of the ferroelectric switching process and dopant-dependent switching properties in orthorhombic HfO_2: A first principles insight, Appl. Phys. Lett. **104**, 092906 (2014).

[10] X. Sang, E. D. Grimley, T. Schenk, U. Schroeder, and J. M. LeBeau, On the structural origins of ferroelectricity in HfO_2 thin films, Appl. Phys. Lett. **106**, 162905 (2015).

[11] P. Fan, Y. K. Zhang, Q. Yang, J. Jiang, L. M. Jiang, M. Liao, and Y. C. Zhou, Origin of the intrinsic ferroelectricity of HfO_2 from ab initio molecular dynamics, J. Phys. Chem. C **123**, 21743 (2019).

[12] L. L. Tao, T. R. Paudel, A. A. Kovalev, and E. Y. Tsymbal, Reversible spin texture in ferroelectric HfO_2, Phys. Rev. B **95**, 245141 (2017).

[13] Q. Yang, L. Tao, Z. Jiang, Y. Zhou, E. Y. Tsymbal, and V. Alexandrov, Magnetoelectric Effect at the Ni/HfO_2 Interface Induced by Ferroelectric Polarization, Phys. Rev. Appl. **12**, 024044 (2019).

[14] S. Liu and B. M. Hanrahan, Effects of growth orientations and epitaxial strains on phase stability of HfO_2 thin films, Phys. Rev. Mater. **3**, 054404 (2019).

[15] S. Estandía, N. Dix, J. Gazquez, I. Fina, J. Lyu, M. F. Chisholm, J. Fontcuberta, and F. Sanchez, Engineering ferroelectric $Hf_{0.5}Zr_{0.5}O_2$ thin films by epitaxial stress, ACS Appl. Electron. Mater. **1**, 1449 (2019).

[16] M. H. Park, Y. H. Lee, H. J. Kim, Y. J. Kim, T. Moon, K. D. Kim, J. Mueller, A. Kersch, U. Schroeder, and T. Mikolajick, Ferroelectricity and antiferroelectricity of doped thin HfO_2-based films, Adv. Mater. **27**, 1811 (2015).

[17] R. Batra, T. D. Huan, G. A. Rossetti Jr, and R. Ramprasad, Dopants promoting ferroelectricity in hafnia: Insights from a comprehensive chemical space exploration, Chem. Mater. **29**, 9102 (2017).

[18] M. Falkowski, C. Künneth, R. Materlik, and A. Kersch, Unexpectedly large energy variations from dopant interactions in ferroelectric HfO_2 from high-throughput ab initio calculations, npj Comput. Mater. **4**, 73 (2018).

[19] Y. Zhou, Y. K. Zhang, Q. Yang, J. Jiang, P. Fan, M. Liao, and Y. C. Zhou, The effects of oxygen vacancies on ferroelectric phase transition of HfO_2-based thin film from first-principle, Comput. Mater. Sci. **167**, 143 (2019).

[20] R. Batra, T. D. Huan, J. L. Jones, G. Rossetti Jr, and R. Ramprasad, Factors favoring ferroelectricity in hafnia: A first-principles computational study, J. Phys. Chem. C **121**, 4139 (2017).

[21] R. Materlik, C. Künneth, and A. Kersch, The origin of ferroelectricity in $Hf_{1-x}Zr_xO_2$: A computational investigation and a surface energy model, J. Appl. Phys. **117**, 134109 (2015).

[22] Y. Wei, P. Nukala, M. Salverda, S. Matzen, H. J. Zhao, J. Momand, A. S. Everhardt, G. Agnus, G. R. Blake, and P. Lecoeur, A rhombohedral ferroelectric phase in epitaxially strained $Hf_{0.5}Zr_{0.5}O_2$ thin films, Nat. Mater. **17**, 1095 (2018).

[23] G. Kresse and D. Joubert, From ultrasoft pseudopotentials to the projector augmented-wave method, Phys. Rev. B **59**, 1758 (1999).

[24] J. P. Perdew, K. Burke, and M. Ernzerhof, Generalized Gradient Approximation Made Simple, Phys. Rev. Lett. **77**, 3865 (1996).

[25] H. J. Monkhorst and J. D. Pack, Special points for Brillouin-zone integrations, Phys. Rev. B **13**, 5188 (1976).
[26] R. King-Smith and D. Vanderbilt, Theory of polarization of crystalline solids, Phys. Rev. B **47**, 1651 (1993).
[27] R. E. Cohen, Origin of ferroelectricity in perovskite oxides, Nature **358**, 136 (1992).
[28] Q. Yang, J. X. Cao, Y. C. Zhou, Y. Zhang, Y. Ma, and X. J. Lou, Tunable oxygen vacancy configuration by strain engineering in perovskite ferroelectrics from first-principles study, Appl. Phys. Lett. **103**, 142911 (2013).
[29] J. C. Boettger, Nonconvergence of surface energies obtained from thin-film calculations, Phys. Rev. B **49**, 16798 (1994).